iki: the inverse Kinematics of $e^+e^- \to t\ \bar{t} \to \mu^+\mu^- b\ \bar{b}\ \nu_\mu\bar{\nu}_\mu$

1 Introduction

The aim of this note is to establish that the kinematics of the process $e^+e^- \to t\ \bar{t} \to \mu^+\mu^- b\ \bar{b}\ \nu_\mu\bar{\nu}_\mu$ can be fully reconstructed from the measurements of the two muons three-momentum and the directions of the two b-jets, despite the two undetected neutrinos, with no ambiguity. The method is termed iki as it amounts to an inversion of the kinematics, from measurement to production.

Three rest frames are used: the ILC rest frame ($\mathcal{R}$) where the measurements are performed; the top rest frame ($\mathcal{R}^*$); and the W^+ rest frame ($\mathcal{R}^{**}$). As shown below, using the direction of the b-jet as determined in $\mathcal{R}$, one can Lorentz Boost the μ^+ momentum into $\mathcal{R}^{**}$ where its energy must be equal to $m_W/2$. This provides a constraint, that, combined with the similar constraint coming from the anti-top decay, fixes completely the kinematics of the final state, up to multiple solutions. The ambiguity for the choice to be made within the multiple solutions is lifted using the b-jets energies.

The discussion focuses on the top decay ($t \to bW^+ \to b\mu^+\nu_\mu$) since the transcription into the anti-top decay is straightforward.

2 ILC rest frame : $\mathcal{R}$

In the ILC rest frame, four-momenta $p = (E, \vec{p}\,)$ are denoted as $t = (E_t, \vec{t}\,)$ (and similarly for b, μ^+, W^+) for the top part, and $\bar{t}$, $\bar{b}$, μ^-, W^- for the anti-top part.

2.1 b-quark

The three-momentum of the ultrarelativistic b quarks can be written as:

$$\vec{b} = \hat{\eta}_b E_b \tag{1}$$

where the direction $\hat{\eta}_b$ is measured, but E_b is assumed to be too poorly measured to be directly used. However, it will be used as an additional, very important constraint.

2.2 Muon

The three-momentum $\vec{\mu}^+$ of the ultrarelativistic μ^+ is assumed to be precisely measured, both direction and energy will be used.

2.3 t-quark

The three-momentum of the top quark is:

$$\vec{t} = \vec{\beta}_t E_t \tag{2}$$

with,

$$\vec{\beta}_t = \beta_t \hat{\beta}_t \tag{3}$$

$$\hat{\beta}_t = (\sin\theta_t \cos\phi_t, \sin\theta_t \sin\phi_t, \cos\theta_t) \tag{4}$$

$$\beta_t = \sqrt{1 - \gamma_t^{-2}} \tag{5}$$

$$\gamma_t = \frac{E_t}{m_t} \tag{6}$$

$$E_t = \frac{\sqrt{S}}{2} \tag{7}$$

The two unknown ϕ_t and θ_t will be fixed through a set of two equations that are derived below. All kinematical quantities can be computed in terms of ϕ_t and θ_t (plus $\hat{\eta}_b$, $\hat{\eta}_{\bar{b}}$, $\vec{\mu}^+$ and μ^-).

2.4 The top rest frame : $\mathcal{R}^*$

For a given pair (ϕ_t, θ_t) the Lorentz Boost $\vec{\beta}_t$ being fixed, one can reach $\mathcal{R}^*$.

2.5 The b quark in the top rest frame

In the top rest frame, for the decay $t \to W^+ b$, the three-momentum of the (massless) b is:

$$\vec{b}^* = \hat{\eta}_b^* E_b^* \tag{8}$$

with:

$$E_b^* = \frac{m_t^2 - m_W^2}{2m_t} \tag{9}$$

The relationship between b directions in $\mathcal{R}^*$ and $\mathcal{R}$ is:

$$\hat{\eta}_b^* = \frac{\vec{b}^*}{E_b^*} = \frac{\hat{\eta}_b + \hat{\beta}_t \Big((\gamma_t - 1)(\hat{\beta}_t \cdot \hat{\eta}_b) - \beta_t \gamma_t \Big)}{\gamma_t \Big(1 - \beta_t (\hat{\beta}_t \cdot \hat{\eta}_b) \Big)} \tag{10}$$

which expresses $\hat{\eta}_b^*$ in terms of the 2 unknown ϕ_t and θ_t.

2.6 The W^+ quark in the top rest frame

In the top rest frame, the W^+ three-momentum is:

$$(\vec{W}^+)^* = (\vec{\beta}_{W^+})^* E_W^* \tag{11}$$

with:

$$(\vec{\beta}_{W^+})^* = \beta_{W^+}^* \hat{\beta}_W^* \tag{12}$$

$$\hat{\beta}_{W^+}^* = -\hat{\eta}_b^* \tag{13}$$

$$\beta_W^* = \sqrt{1 - (\gamma_W^*)^{-2}} \tag{14}$$

$$\gamma_W^* = \frac{E_W^*}{m_W} \tag{15}$$

$$E_W^* = \frac{m_t^2 + m_W^2}{2m_t} \tag{16}$$

2.7 The μ^+ in the top rest frame

Similarly, the three-momentum of the (massless) μ^+ in the top rest frame is given by:

$$(\vec{\mu}^+)^* = \vec{\mu}^+ + \hat{\beta}_t \Big((\gamma_t - 1)(\hat{\beta}_t \cdot \vec{\mu}^+) - \beta_t \gamma_t E_{\mu^+} \Big) \tag{17}$$

where $E_{\mu^+} = \mid \vec{\mu}^+ \mid$. In particular, its energy is:

$$E_{\mu^+}^* = \gamma_t (E_{\mu^+} - \beta_t (\hat{\beta}_t \cdot \vec{\mu}^+)) \tag{18}$$

3 The W^+ rest frame : $\mathcal{R}^{**}$

3.1 The μ^+ in the W^+ rest frame

In the W^+ rest frame, the energy of the μ^+ must satisfy:

$$\frac{m_W}{2} = E_{\mu^+}^{**}(\phi_t, \theta_t) \equiv \gamma_W^* (E_{\mu^+}^* - \beta_W^* (\hat{\beta}_W^* \cdot (\vec{\mu}^+)^*)) \tag{19}$$

where $(\vec{\mu}^+)^*$ is given by Eq.(17), $E_{\mu^+}^*$ by Eq.(18) and $(-\hat{\beta}_W^*)$ by Eq.(10).

4 The two kinematical constraints

One can repeat the above reasoning for the anti-top decay to obtain the set of two constraints:

$$\frac{m_W}{2} = \gamma_W^*(E_{\mu^+}^* - \beta_W^*(\hat{\beta}_W^* \cdot (\vec{\mu}^+)^*)) \quad (20)$$

$$\frac{m_W}{2} = \gamma_W^*(E_{\mu^-}^* - \beta_W^*(\hat{\beta}_W^* \cdot (\vec{\mu}^-)^*)) \quad (21)$$

where the second equation is derived from the first by the change of variables: $E_{\mu^+} \to E_{\mu^-}$, $\hat{\eta}_b \to \hat{\eta}_{\bar{b}}$, $\beta_t \to -\beta_t$. This set of two equations being non-linear it involves multiple solutions (typically two, it seems): an example is illustrated on Fig.(1), for $\sqrt{S} = 500$ GeV. These multiple solutions are further amplified when one exchanges the role ot b and $\bar{b}$ (assuming that the charge of the b-jets are not determined experimentally).

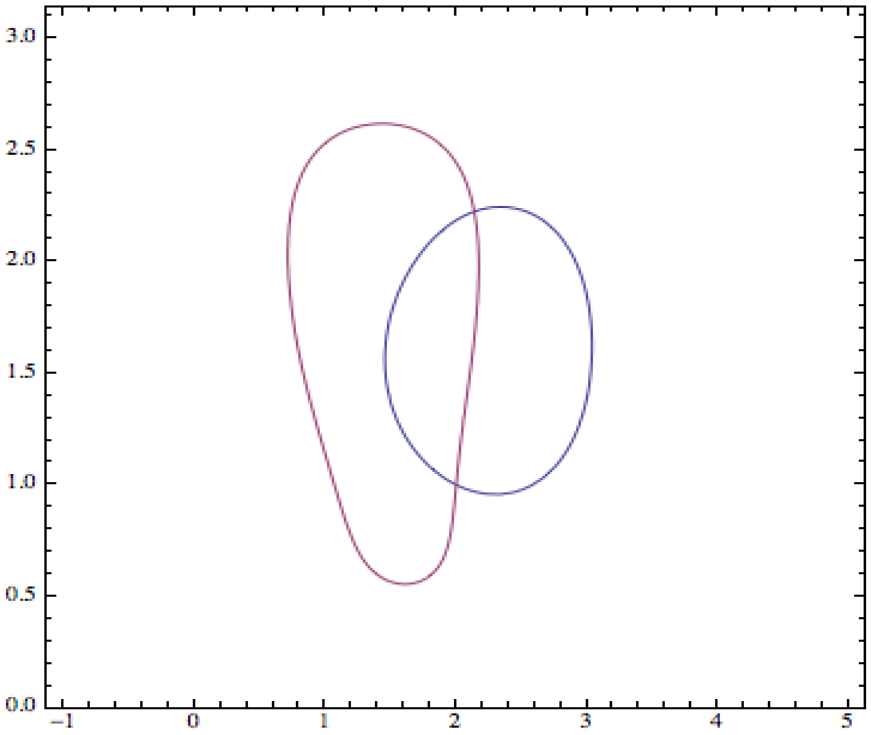

Figure 1: The plan ϕ_t (horizontal axis) θ_t (vertical axis). The two close curves represent the solutions of the two constraints Eq.(20) and Eq.(21). In this example, the curves cross each other in two points which are therefore solutions of the set of two equations. The input (truth) values are $\phi_t = 2$ and $\theta_t = 1$.

5 The measurements of the b-jet energies

To select the right solution, one can make use of the measurement of the b-jet energies as follows: for a given pair (ϕ_t, θ_t), one can compute the complete kinematics of the events. In particular, the reconstructed b and $\bar{b}$ energies in $\mathcal{R}$ are obtained as:

$$E_b^{\rm rec}(\phi_t, \theta_t) = \gamma_t E_b^*(1 + \beta_t(\hat{\beta}_t \cdot \hat{\eta}_b^*)) \quad (22)$$

$$E_{\bar{b}}^{\rm rec}(\phi_t, \theta_t) = \gamma_t E_b^*(1 - \beta_t(\hat{\beta}_t \cdot \hat{\eta}_b^*)) \quad (23)$$

with:

$$\hat{\eta}_{\bar{b}}^* = \frac{\hat{\eta}_{\bar{b}} + \hat{\beta}_t\left((\gamma_t - 1)(\hat{\beta}_t \cdot \hat{\eta}_b) + \beta_t\gamma_t\right)}{\gamma_t\left(1 + \beta_t(\hat{\beta}_t \cdot \hat{\eta}_b)\right)} \quad (24)$$

With these energies, one can form the χ^2:

$$\chi^2_b(\phi_t,\theta_t) = \left(\frac{E_b - E^{\rm rec}_b(\phi_t,\theta_t)}{\sigma_j\sqrt{E_b}}\right)^2 + \left(\frac{E_{\bar{b}} - E^{\rm rec}_{\bar{b}}(\phi_t,\theta_t)}{\sigma_j\sqrt{E_{\bar{b}}}}\right)^2 \tag{25}$$

where $\sigma_j \simeq 0.3$ (from ILC detector simulations). One can consider only the regions in the (ϕ_t,θ_t) plane that are not excluded at 99% CL, that is to say with $\chi^2_b < 9.2$, and search there for solution(s) of two constraints Eq.(20) and Eq.(21). The shape of these regions can be intricate, but may also be simple ellipses, depending on the event at hand.

This constraint becomes blunt when approaching the $t\bar{t}$ production threshold: when $\mathcal{R}^*$ gets close to $\mathcal{R}$: then $E^{\rm rec}_{\bar{b}}(\phi_t,\theta_t) \simeq E^*_b$, i.e. (ϕ_t,θ_t) drops out and the above function tends to vanish in the whole (ϕ_t,θ_t) plane. However, the constraint sharpens quickly with increasing energy, as illustrated by Fig.(3).

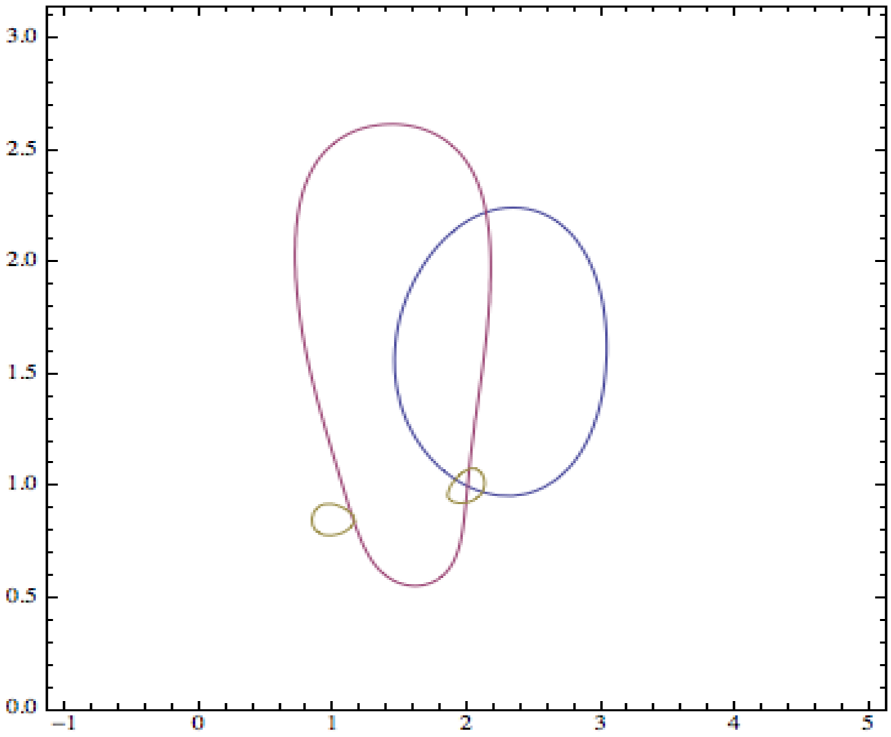

Figure 2: The plan ϕ_t (horizontal axis) θ_t (vertical axis). The two close curves are the ones of Fig.(1). The two additional ellipsoidal contours delimit regions which are not excluded at 99%CL, i.e. where $\chi^2 < 9.2$. The input values (i.e. $\phi_t = 2$ and $\theta_t = 1$) are unambiguously selected by this additional constraint.

6 The measurements of the Muon energies

To restore a symmetrical between the b and the μ^+, it is useful to compute $E^{\rm rec}_{\mu^+}$, the three-momentum of the muon in $\mathcal{R}$. Since the muon mass is neglected, a factor applied to a E_{μ^+} in any rest frame applies in the same way in any rest frame. Hence, imposing that in $\mathcal{R}^{**}$ the μ^+ energy is equal to $m_W/2$ implies in turn that the corresponding μ^+ energy should be, in $\mathcal{R}$:

$$E^{\rm rec}_{\mu^+}(\phi_t,\theta_t) \quad = \quad \frac{\frac{m_W}{2}}{E^{**}_{\mu^+}(\phi_t,\theta_t)} E_{\mu^+} \tag{26}$$

In the ILC rest frame the measurement of the μ^+ energy E_{μ^+} is deduced from the measurement of the inverse of its transverse momentum:

$$\frac{1}{(p_{\mu^+})_\perp} = \frac{1}{E_{\mu^+}\sin\theta_{\mu^+}} \tag{27}$$

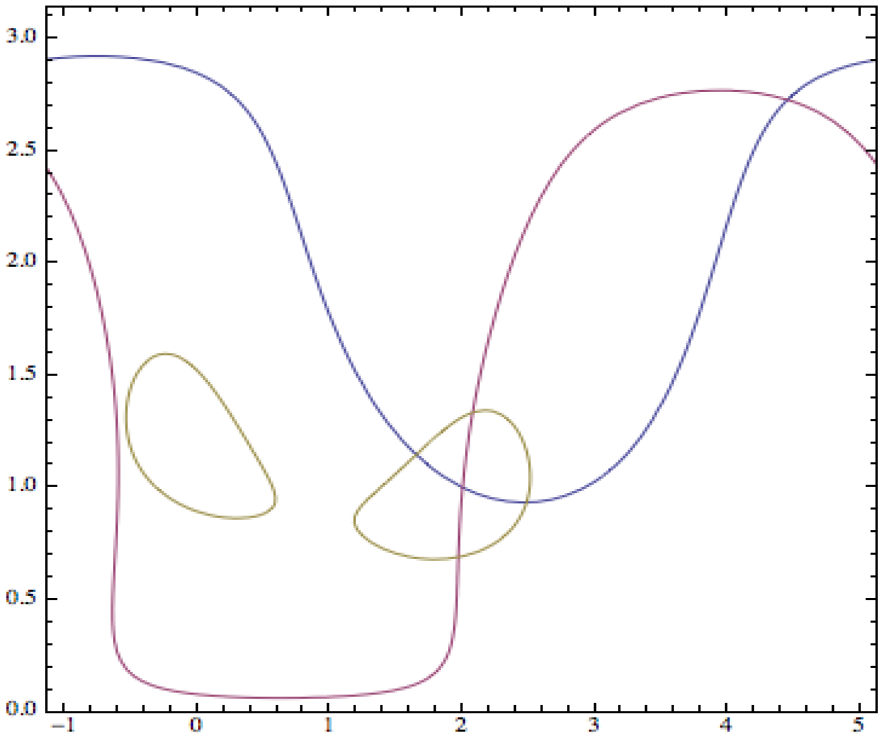

Figure 3: The plan ϕ_t (horizontal axis) θ_t (vertical axis). The two close curves correspond to the ones of Fig.(1), using the same input values except for $\sqrt{S} = 360$ GeV (instead of 500 GeV). The two additional ellipsoidal contours delimit regions which are not excluded at 99%CL, i.e. where $\chi^2 < 9.2$. Although being close to threshold, he input values ($\phi_t = 2$ and $\theta_t = 1$) are still unambiguously selected by the b-energy constraint.

the latter being obtained with a Gaussian resolution (in GeV^{-1}, cf. TDR volume 4 page 285 (for ILD)):

$$\sigma[\frac{1}{p_\perp}] = 2\ 10^{-5} \oplus 10^{-3} \frac{1}{p_\perp \sin\theta} \tag{28}$$

The corresponding χ^2 component is thus:

$$\chi^2_{\mu^+} = \left((\frac{1}{(p_{\mu^+})_\perp} - \frac{1}{(p_{\mu^+})^{\text{rec}}_\perp}) \frac{1}{\sigma[\frac{1}{p_\perp}]} \right)^2 \tag{29}$$

with

$$\frac{1}{(p_{\mu^+})^{\text{rec}}_\perp} = \frac{1}{E^{\text{rec}}_{\mu^+} \sin\theta_{\mu^+}} = \frac{E^{**}_{\mu^+}(\phi_t, \theta_t)}{\frac{m_W}{2}} \frac{1}{(p_{\mu^+})_\perp} \tag{30}$$

and hence: The corresponding χ^2 component is thus:

$$\chi^2_{\mu^+} = \left(\frac{1}{(p_{\mu^+})_\perp} (1 - \frac{E^{**}_{\mu^+}(\phi_t, \theta_t)}{\frac{m_W}{2}}) \frac{1}{\sigma[\frac{1}{p_\perp}]} \right)^2 \tag{31}$$

$$= \left((\frac{m_W}{2} - E^{**}_{\mu^+}(\phi_t, \theta_t)) \frac{m_W}{2(p_{\mu^+})_\perp \sigma[\frac{1}{p_\perp}]} \right)^2 \tag{32}$$

$$= \left(\frac{\frac{m_W}{2} - E^{**}_{\mu^+}(\phi_t, \theta_t)}{\sigma[E^{**}_{\mu^+}]} \right)^2 \tag{33}$$

where the uncertainty in the denominator is defined as:

$$\sigma[E^{**}_{\mu^+}] = \frac{2(p_{\mu^+})_\perp \sigma[\frac{1}{p_\perp}]}{m_W} \tag{34}$$

7 Technical Procedure

Technically, to locate the optimal solution, one could proceed as follows:

1- χ^2_μ : it is defined from Eq.(33)

$$\chi^2_\mu(\phi_t, \theta_t) = \chi^2_{\mu^+} + \chi^2_{\mu^-} \tag{35}$$

2- Compound χ^2 ($\chi^2_{\rm tot}$):
One minimizes the compound χ^2:

$$\chi^2_{\rm tot} = \chi^2_\mu(\phi_t, \theta_t) + \chi^2_b(\phi_t, \theta_t) \tag{36}$$

for the two hypotheses for b and $\bar{b}$. The best of the two χ^2 is selected. It should be close to two (2 degrees of freedom) for the right combination, while the second combination should yield a large $\chi^2_{\rm tot}$, as illustrated in Fig.(4). The retained solution provides either:

- the final solution, if one is willing to use the expected statistical uncertainty on the measurements of the b-jet energies (in that case one may also apply Breit-Wigner constraints on the top's and the W's),
- or a seed for ϕ_t and θ_t, using in a final step a simplified χ^2 where the b-jet energies do not appear any more. Starting from this seed, one removes $\chi^2_b(\phi_t, \theta_t)$ and minimizes:

$$\chi^2_{\rm iki} = \left(E^{**}_{\mu^+} - \frac{m_W}{2}\right)^2 + \left(E^{**}_{\mu^-} - \frac{m_W}{2}\right)^2 \tag{37}$$

to locate the final solution, for which $\chi^2_{\rm iki}$ should be strictly zero.

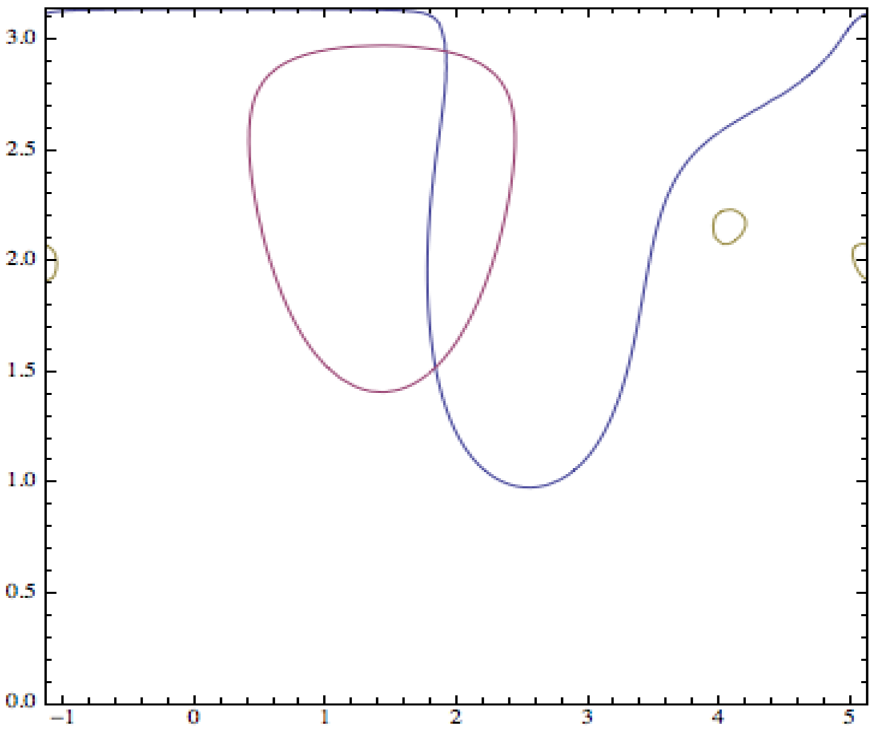

Figure 4: The plan ϕ_t (horizontal axis) θ_t (vertical axis). The two curves correspond to the ones of Fig.(1), using the same input values except that one uses the $\bar{b}$ jet direction for the top reconstruction, and conversely for the anti-top reconstruction. The contours are completely changed, but the b-energy constraint totally excludes this combination.

8 Systematical effects

8.1 Widths

The effect of the top and W widths appears small, as illustrated by Fig.(5) where at generation level the t, W^+, $\bar{t}$ and W^- masses were all reduced by 3 times their respective widths. In this example, the solution is found to be $\phi = 2.06$ and $\theta = 0.92$, very close to the input values $\phi = 2.$ and $\theta = 1.$.

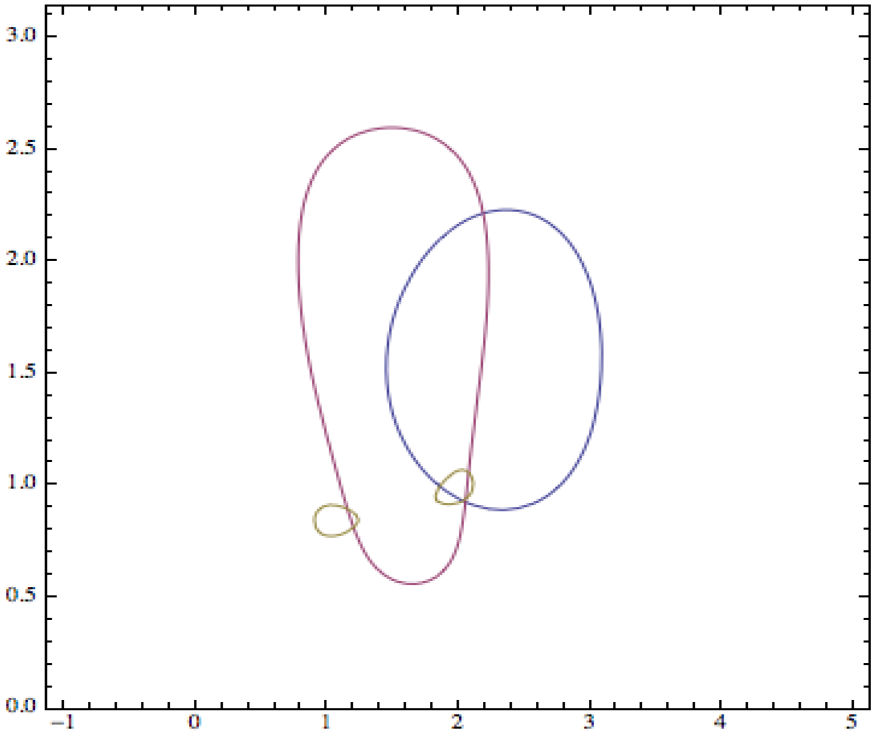

Figure 5: The plan ϕ_t (horizontal axis) θ_t (vertical axis). The two close curves correspond to the ones of Fig.(1), using the same input values except the top quarks and W bosons masses which are all reduced by 3 times their respective width. The three contours are only slightly shifted, but the procedure advocated in the previous section will pick up the best solution, which is close to the truth, although it is no longer within the 99%CL allowed region.